Highly-efficient Reduced Order Modelling Techniques for Shallow Water Problems

D.A. Bistrian and I.M. Navon

Department of Electrical Engineering and Industrial Informatics, University Politehnica of Timisoara, Romania,
Department of Scientific Computing, Florida State University, USA

International Conference on Applied Sciences (ICAS2017), May 10-12, 2017, Faculty of Engineering Hunedoara, Hunedoara, Romania

Outline

Motivation of Reduced Order Modelling

- The modal decomposition of fluid dynamics is a frequently employed technique, capable of providing tools for studying dominant and coherent structures in turbulent flows.

- A complex turbulent flow often consists of a superposition of coherent structures, whose development is responsible for the bulk mass, energy transfer or hydrodynamic instability.

- The present study is motivated by the need to further clarify the connection between Koopman modes and POD dynamic modes, as well as address their physical significance, for problems occurring in oceanography.

Reduced Order Modelling (ROM) Principles

Dimension reduction means representing the solution of a dynamical system in high dimensional space $w \in \mathbb{R}^n$ with a corresponding vector in a much lower dimensional space $\widetilde{w} \in \mathbb{R}^p$, $p \ll n$, assuring:

(i) Preservation of stability,

(ii) Computational stability and efficiency,

(iii) Approximation error small-global error bounded.

Complementary techniques for ROM

- Proper orthogonal decomposition (POD) finds the most persistent spatial structures Φ_j^{POD} and is primarily limited to flows whose coherent structures can be hierarchically ranked in terms of their energy content.

$$w(x, y, t) \approx \sum_{j=1}^{p} \underbrace{b_j^{POD}(t)}_{Amplitudes} \underbrace{\Phi_j^{POD}(x, y)}_{Spatial\ modes},$$

- Dynamic Mode Decomposition (DMD) finds the single frequency modes ϕ_j^{DMD} and approximates the eigenvalues of the Koopman operator.

$$w(x, y, t) \approx \sum_{j=1}^{r} \underbrace{a_j^{DMD}}_{Amplitude} \underbrace{e^{\lambda_j t}}_{Time\ evolution} \underbrace{\phi_j^{DMD}(x, y)}_{Spatial\ modes}$$

Saint–Venant Equations (Shallow Water Equations)

In the Cartesian coordinates formulation, we suppose there exists a time dependent flow $w = (u, v, h)(x, y, t) \in \mathbb{V}$ and a given initial flow $w(x, y, 0) = (u_0, v_0, h_0)(x, y)$, that are solutions of the Saint Venant equations, also called the Shallow Water Equations (SWE),

$$u_t + uu_x + vu_y + \eta_x - fv = 0, \tag{1}$$

$$v_t + uv_x + vv_y + \eta_y + fu = 0, \tag{2}$$

$$\eta_t + (\eta u)_x + (\eta v)_y = 0, \tag{3}$$

where $u(x, y, t)$ and $v(x, y, t)$ are the velocity components in the x and y axis respectively, $\eta(x, y, t) = gh(x, y, t)$ is the geopotential height, $h(x, y, t)$ represents the depth of the fluid, f is the Coriolis factor and g is the acceleration of gravity.

Boundary conditions:

$$w\left(0, y, t\right) = w\left(L_{\max}, y, t\right), \ v\left(x, 0, t\right) = v\left(x, D_{\max}, t\right) = 0. \tag{4}$$

The initial Grammeltvedt condition I1 as the initial height field:

$$h_0\left(x, y\right) = H_0 + H_1 \tanh\left(\frac{9(D_{\max}/2 - y)}{2D_{\max}}\right) + H_2 \sin\left(\frac{2\pi x}{L_{\max}}\right) \cosh^{-2}\left(\frac{9(D_{\max}/2 - y)}{D_{\max}}\right), \tag{5}$$

The initial velocity fields using the geostrophic relationship, $u = -h_y\left(g/f\right)$, $v = h_x\left(g/f\right)$:

$$u_0\left(x, y\right) = -\frac{g}{f}\frac{9H_1}{2D_{\max}}\left(\tanh^2\left(\frac{9D_{\max}/2 - 9y}{2D_{\max}}\right) - 1\right) -$$

$$\frac{18g}{f}H_2 \sinh\left(\frac{9D_{\max}/2 - 9y}{D_{\max}}\right)\frac{\sin\left(\frac{2\pi x}{L_{\max}}\right)}{D_{\max}\cosh^3\left(\frac{9D_{\max}/2 - 9y}{D_{\max}}\right)}, \tag{6}$$

$$v_0\left(x, y\right) = 2\pi H_2 \frac{g}{fL_{\max}}\cos\left(\frac{2\pi x}{L_{\max}}\right)\cosh^{-2}\left(\frac{9(D_{\max}/2 - y)}{D_{\max}}\right). \tag{7}$$
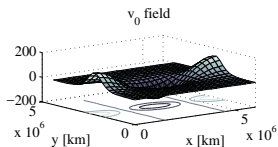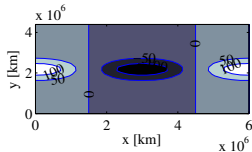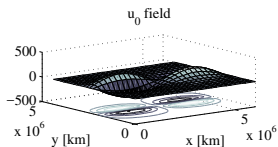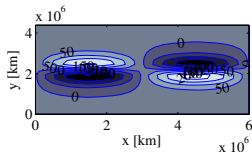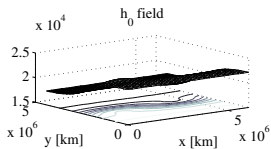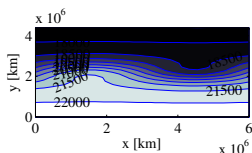
Figure: Initial velocity fields: Geopotential height field for the Grammeltvedt initial condition h_0, streamwise and spanwise velocity fields (u_0, v_0) calculated from the geopotential field by using the geostrophic approximation.

$$w(x, y, t) \approx \sum_{j=1}^{p} \underbrace{b_j^{POD}(t)}_{\textit{Amplitudes}} \underbrace{\Phi_j^{POD}(x, y)}_{\textit{Spatial modes}},$$

- POD is related to the principal component analysis, Karhunen-Love expansion in the stochastic process theory, and the method of empirical orthogonal functions.
- POD represents at the moment state-of-the-art technique for the reduced-order modeling of nonlinear PDEs.
- The strong point of POD is that it can be applied to non-linear partial differential equations, especially for smooth systems in which the energetics can be characterized by the first few modes.
- Related work: Holmes et al. 1996 [7], Navon and DeVilliers 1996 [2], Fang et al. 2009 [5], Wang et al. 2012 [6], Stefanescu and Navon 2013 [4].

Description of POD Method

- POD approximates the state variable as a finite sum of form

$$w(x, y, t) \approx \sum_{j=1}^{p} b_j(t) \Phi_j(x, y), \qquad (8)$$

  expecting that this approximation becomes exact as $p \to +\infty$.

- The POD problem reduces to find the subspace
  $X = span\{\Phi_1, \Phi_2, ..., \Phi_p\}$ spanned by the sequence of orthonormal
  functions $\Phi_j(x, y)$ such that the p-approximation of $w(x, y, t)$ is as good
  as possible in the least square sense:

$$\min_{\Phi_1, \Phi_2, ..., \Phi_p} \int_{\Omega} \left\| w(x, y, t) - \sum_{j=1}^{p} \langle w(x, y, t), \Phi_j(x, y) \rangle_{L^2} \Phi_j(x, y) \right\|_{L^2}^2 dr$$
$$s.t. \quad \langle \Phi_i, \Phi_j \rangle_{L^2} = \delta_{ij}, \ 1 \le i \le j \le p$$

$$(9)$$

POD Algorithm for 2D flows

(i) Collect data $w_i(x, y) = w(x, y, t_i)$, $t_i = i\Delta t$, $i = 0, ..., N$ from the flow field, equally distributed in time.

(ii) Placing the columns one after another, transform snapshots w_i into columns $\widetilde{w}_i$ of the matrix

$$\mathcal{V} = \begin{bmatrix} \widetilde{w}_0 & \widetilde{w}_1 & ... & \widetilde{w}_N \end{bmatrix}. \tag{10}$$

(iii) Compute the mean column $\overline{W}_b = \frac{1}{N+1} \sum_{i=0}^{N} \widetilde{w}_i$ and the mean-subtracted snapshot matrix $\mathcal{V}' = \mathcal{V} - \overline{W}_b$. Reshaping $\overline{W}_b$ into the matrix form corresponds to the base flow $W_b(x, y)$.

POD Algorithm for 2D flows

(iv) Calculate the empirical correlation matrix

$$C = \frac{1}{N+1} \mathcal{V}' \mathcal{V}'^{T}, \tag{11}$$

where $N+1$ represents the number of snapshots and $\mathcal{V}'^{T}$ represents the transpose of the mean subtracted snapshot matrix.

(v) Compute the singular eigenvalue decomposition

$$C v_j = \lambda_j v_j, \quad j = 1, ..., N+1, \quad v_j \in \mathbb{R}^{N+1}, \tag{12}$$

where $N+1$ represents the number of the total eigenvalues.

(vi) Find the number of POD basis vectors r_{POD} capturing 99.99% of the snapshots energy, defined as

$$e_{POD} = \sum_{j=1}^{r_{POD}} \lambda_j \left/ \sum_{j=1}^{N+1} \lambda_j \right. . \tag{13}$$

POD Algorithm for 2D flows

(vii) We can choose the first orthonormal basis of eigenvectors $\{v_1, ..., v_{r_{POD}}\}$ and the corresponding POD basis functions are given by

$$\Phi_j = \frac{1}{\sqrt{\lambda_j}} \mathcal{V}' v_j, \quad j = 1, ..., r_{POD}. \tag{14}$$

(viii) The temporal coefficients are stored in the matrix B, which is obtained by relation

$$B = \Phi^T \mathcal{V}'. \tag{15}$$

POD-ROM Model

- Full model:

$$\begin{cases} \frac{\partial w}{\partial t}(x, y, t) = f(t, w(x, y, t)) \\ w(x, y, t_0) = w_0(x, y) \end{cases} \tag{16}$$

- POD approximation:

$$w(x, y, t) \approx w^{POD}(x, y, t) = W_b(x, y) + \sum_{j=1}^{r_{POD}} b_j(t) \Phi_j(x, y), \tag{17}$$

- Galerkin projection gives the POD-ROM and allows reconstruction of reduced order model by solving the resulting ODE system:

$$\dot{b}_i(t) = \sum_{m=1}^{r_{POD}} \sum_{n=1}^{r_{POD}} d_{imn} b_m(t) b_n(t) + \sum_{m=1}^{r_{POD}} d_{im} b_m(t), \quad i = 1, ..., r_{POD}. \tag{18}$$

$$\dot{b}_i(t) = \left\langle \Phi_i(\cdot), f\left(t, \sum_{j=1}^{r_{POD}} \Phi_j(\cdot) b_j(t)\right) \right\rangle, \tag{19}$$

with the initial condition

$$b_i(t_0) = \langle \Phi_i(\cdot), w_0 \rangle, \text{ for } i = 1, ..., r_{POD}. \tag{20}$$

Description of DMD Method

$$w(x, y, t) \approx \sum_{j=1}^{r} \underbrace{a_j^{DMD}}_{Amplitude} \underbrace{e^{\lambda_j t}}_{Time\ evolution} \underbrace{\phi_j^{DMD}(x, y)}_{Spatial\ modes}$$

- Introduced by Rowley in 2009 [5] for spectral analysis of nonlinear flows.
- In 2010, Schmid [1] recommends an alternate algorithm, based on averaging the mapping from the snapshots to the new one, upon which the work within this article is based.
- Related work: Rowley 2009 [5], Schmid 2010 [1], Bagheri 2013 [3], Mezic 2013 [4], Belson et al. 2014 [6].

The Koopman Operator and the General Description of DMD

Considering a dynamical system evolving on a manifold $\mathbb{M}$ such that, for all $w_k \in \mathbb{M}$

$$w_{k+1} = f(w_k), \tag{21}$$

the Koopman operator, defined by Koopman [2] in 1931 maps any scalar-valued function $g : \mathbb{M} \to \mathbb{R}$ into a new function Ug given by

$$Ug\left(w\right) = g\left(f\left(w\right)\right). \tag{22}$$

The Koopman operator is infinite-dimensional and it steps forward in time an observable.

The Koopman Operator and the General Description of DMD

There is a unique expansion that expands each snapshot in terms of vector coefficients ϕ_j which are called Koopman modes and mode amplitudes $a_j(w)$, such that iterates of w_0 are then given by

$$g(w_k) = \sum_{j=1}^{\infty} \lambda_j^k a_j(w_0) \phi_j, \quad \lambda_j = e^{\sigma_j + i\omega_j}, \tag{23}$$

where λ_j are called the Ritz eigenvalues of the modal decomposition, that are complex-valued flow structures associated with the growth rate σ_j and the frequency ω_j.

The Koopman Operator and the General Description of DMD

Assuming that $\{w_0, w_1, ... w_N\}$ is a data sequence collected at a constant sampling time Δt, we define the following matrices

$$V_0^{N-1} = \begin{pmatrix} w_0 & w_1 & ... & w_{N-1} \end{pmatrix}, \quad V_1^N = \begin{pmatrix} w_1 & w_2 & ... & w_N \end{pmatrix}. \quad (24)$$

The DMD algorithm is based on the hypothesis that a Koopman operator $\mathcal{A}$ exists, that steps forward in time the snapshots, such that

$$w_{i+1} = \mathcal{A}w_i, \quad i = 0, ..., N - 1. \quad (25)$$

It follows that the snapshots data set

$$V_0^{N-1} = \begin{pmatrix} w_0 & \mathcal{A}w_0 & \mathcal{A}^2 w_0 & ... & \mathcal{A}^{N-1}w_0 \end{pmatrix} \quad (26)$$

corresponds to the Nth Krylov subspace generated by the Koopman operator from w_0.

The Koopman Operator and the General Description of DMD

For a sufficiently long sequence of the snapshots, we suppose that the last snapshot w_N can be written as a linear combination of previous $N - 1$ vectors, such that

$$w_N = c_0 w_0 + c_1 w_1 + ... + c_{N-1} w_{N-1} + \mathcal{R}, \tag{27}$$

which can be written in matrix notation as

$$w_N = V_0^{N-1} c + \mathcal{R} e_{N-1}^T, \tag{28}$$

in which $c^T = \begin{pmatrix} c_0 & c_1 & ... & c_{N-1} \end{pmatrix}$ is a complex column vector and $\mathcal{R}$ is the residual vector.

The Koopman Operator and the General Description of DMD

We assemble the following relations

$$\mathcal{A}\{w_0, w_1, ... w_{N-1}\} = \{w_1, w_2, ... w_N\} = \left\{w_1, w_2, ... V_0^{N-1}c\right\} + \mathcal{R}e_{N-1}^T \quad (29)$$

in the matrix notation form,

$$\mathcal{A}V_0^{N-1} = V_1^N = V_0^{N-1}\mathcal{C} + \mathcal{R}e_{N-1}^T, \quad \mathcal{C} = \begin{pmatrix} 0 & ... & 0 & c_0 \\ 1 & & 0 & c_1 \\ \vdots & \vdots & \vdots & \vdots \\ 0 & \ldots & 1 & c_{N-1} \end{pmatrix}, \quad (30)$$

where $\mathcal{C}$ is the companion matrix and e_j^T represents the jth Euclidean unitary vector. The last column of the companion matrix may be found using the Moore-Penrose pseudo-inverse of V_0^{N-1}, as

$$c = \left(V_0^{N-1}\right)^+ w_N = \left(\left(V_0^{N-1}\right)^* V_0^{N-1}\right)^{-1} \left(V_0^{N-1}\right)^* w_N.$$

Description of an Improved DMD Algorithm for SWE

The main objective is to find a representation of the flow field in the form

$$w^{DMD}(x, y, t) = W_b + \sum_{j=1}^{r} a_j e^{(\sigma_j + i\omega_j)t} \phi_j(x, y), \tag{31}$$

$$\sigma_j = \frac{\log(|\lambda_j|)}{\Delta t}, \quad \omega_j = \frac{\arg(|\lambda_j|)}{\Delta t}, \tag{32}$$

- $\phi_j \in \mathbb{C}$ are the DMD modes,
- r is the number of the DMD modes kept for flow decomposition,
- $a_j \in \mathbb{C}$ are the amplitudes of the modes,
- $\lambda_j \in \mathbb{C}$ are the Ritz eigenvalues,
- σ_j is the growth rate,
- ω_j is the frequency,
- W_b is a constant offset that represents the data mean, usually called the *base flow*.

Description of an Improved DMD Algorithm

- Selection of modes – is subject of many discussions in literature (Bagheri [3], Mezic [4], Rowley et al. [5], Belson et al. [6], Holmes et al. [7]).
- We introduce in this paper a DMD based approach yielding a supplementary subroutine for extracting the optimal Koopman modes.

Strategy for the Optimal Selection of the Dominant Koopman Modes

We seek for a number $r_{DMD} < r$, which represents the optimal number of the selected modes that must be identified such that the flow can be reconstructed using the first r_{DMD} optimal Koopman modes and associated amplitudes and Ritz eigenvalues as:

$$w^{DMD}(x, y, t) = W_b(x, y) + \sum_{j=1}^{r_{DMD}} a_j \lambda_j \phi_j(x, y). \tag{33}$$

- The DMD algorithm that we propose, is based on the conservation of quadratic integral invariants of the SWE model by the finite-element discretization scheme of the shallow-water model (1)-(3) (Navon 1987 [1]).
- We assume that the reduced order reconstructed flow (33) also preserves the conservation of the total flow energy.
- In parallel, we aim to eliminate the modes that contribute weakly to the data sequence.

Optimal Selection of the Dominant Koopman Modes in DMD

(i) Compute the total energy of the high fidelity flow (Navon 1987 [1])

$$E = \frac{1}{N+1} \sum_{i=0}^{N} \int \int_{\Omega} h_i(x, y) \left(u_i(x, y)^2 + v_i(x, y)^2 \right) + g h_i(x, y)^2 dx\, dy, \quad (34)$$

(ii) Compute the total energy of the reduced order flow

$$E^{DMD} = \frac{1}{N+1} \sum_{i=0}^{N} \int \int_{\Omega} h_i^{DMD}(x, y) \left(u_i^{DMD}(x, y)^2 + v_i^{DMD}(x, y)^2 \right) + g h_i^{DMD}(x, y)^2 dx\, dy, \quad (35)$$

where $(h_i, u_i, v_i)(x, y)$ and $\left(h_i^{DMD}, u_i^{DMD}, v_i^{DMD} \right)(x, y)$, $i = 0, ..., N$ represents the full rank flow, respectively the Koopman decomposed flow at time i.

Optimal Selection of the Dominant Koopman Modes in DMD

(iii) Arrange the Koopman modes in descending order of the energy of the modes, weighted by the inverse of the Strouhal number $St = \arg(\lambda_j) / (2\pi\Delta t)$:

$$e_j^{DMD} = \frac{1}{St} \cdot \frac{\|\phi_j(x,y)\|_F}{\|\mathcal{V}\|_F}, \quad j = 1, ..., r. \tag{36}$$

(iv) Find the solution to the following minimization problem

$$\begin{cases} \underset{r_{DMD}}{Minimize} & \frac{1}{N+1} \sum_{i=0}^{N} \frac{\|w_i(x,y) - w_i^{DMD}(x,y)\|_F}{\|w_i(x,y)\|_F}, \\ Subject\ to & \left|E - E^{DMD}\right| < \varepsilon, \end{cases} \tag{37}$$

where $w_i(x, y)$ and $w_i^{DMD}(x, y)$, $i = 0, ..., N$ represents the full rank flow, respectively the Koopman decomposed flow at time i and $\varepsilon = 10^{-5}$ sets an upper bound on the relative error due to rounding in floating point arithmetic.

DMD-ROM Model

- Full model:

$$\begin{cases} \frac{\partial w}{\partial t}(x,y,t) = f(t, w(x,y,t)) \\ w(x,y,t_0) = w_0(x,y) \end{cases} \tag{38}$$

- DMD approximation:

$$w(x,y,t) \approx w^{DMD}(x,y,t) = W_b(x,y) + \sum_{j=1}^{r_{DMD}} a_j(t) \lambda_j \phi_j(x,y), \tag{39}$$

- Galerkin projection gives the DMD-ROM and allows reconstruction of reduced order model by solving the resulting ODE system:

$$\dot{a}_i(t) = \sum_{m=1}^{r_{DMD}} \sum_{n=1}^{r_{DMD}} c_{imn} a_m(t) a_n(t) + \sum_{m=1}^{r_{DMD}} c_{im} a_m(t), \quad i = 1, ..., r_{DMD}, \tag{40}$$

$$\dot{a}_i(t) = \left\langle \phi_i(\cdot), f\left(t, \sum_{j=1}^{r_{DMD}} \lambda_j \phi_j(\cdot) a_j(t)\right) \right\rangle, \tag{41}$$

with the initial condition

$$a_i(t_0) = \langle \phi_i(\cdot), w_0 \rangle, \text{ for } i = 1, ..., r_{DMD}. \tag{42}$$

Numerical Results for the Improved DMD Algorithm

Setup for the first numerical experiment:

$$D_{max} = 4400km, \quad L_{max} = 6000km,$$

$$\widehat{f} = 10^{-4}s^{-1}, \quad \beta = 1.5 \times 10^{-11}s^{-1}m^{-1}, \quad g = 10ms^{-1},$$

$$H_0 = 2000m, \quad H_1 = 220m, \quad H_2 = 133m,$$

$$\Delta t = 600s, \quad N = 240$$

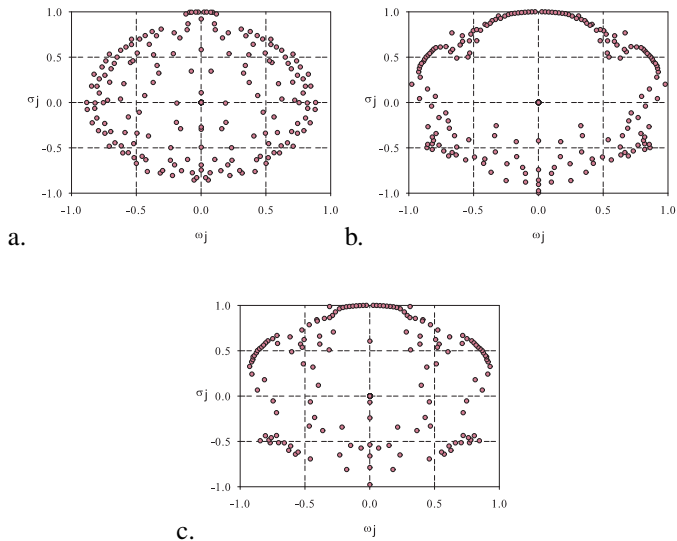unsteady solutions of the two-dimensional shallow water equations model.

Figure: Spectrum of the Dynamic Mode Decomposition: a. Geopotential field *h*; b. Streamwise velocity field *u*; c. Spanwise velocity field *v*, $\Delta t = 600s$.
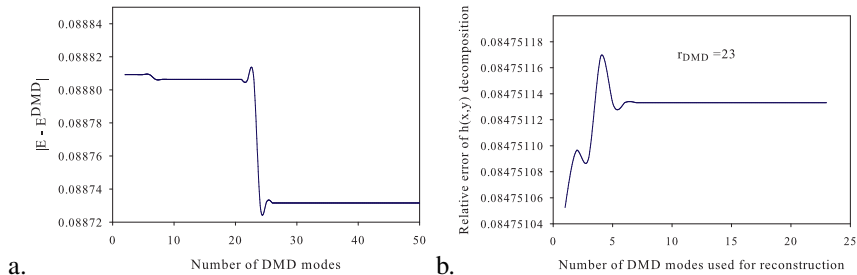
Improved DMD algorithm
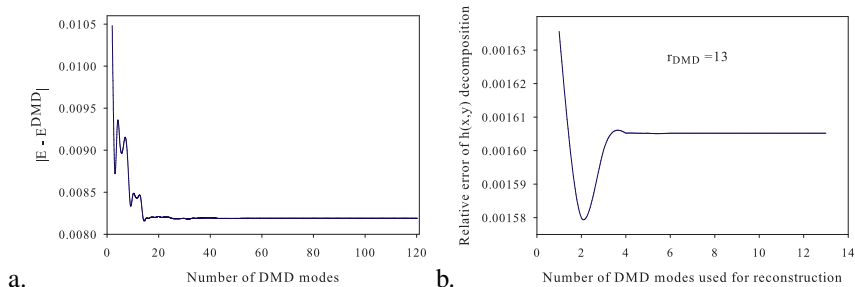
Figure: a. Absolute error between the total energy of the high fidelity flow and the total energy of the reduced order flow, as the number of the DMD modes; b. The relative error $\frac{\left\| h(x,y) - h^{DMD}(x,y) \right\|_E}{\left\| h(x,y) \right\|_F}$ of geopotential height field decomposition, using $r_{DMD} = 13$ modes.

Figure: a. Absolute error between the total energy of the high fidelity flow and the total energy of the reduced order flow, as the number of the DMD modes; b. The relative error $\frac{\left\|h(x,y)-h^{DMD}(x,y)\right\|_E}{\|h(x,y)\|_F}$ of geopotential height field decomposition, using $r_{DMD} = 23$ modes.

Number of basis functions
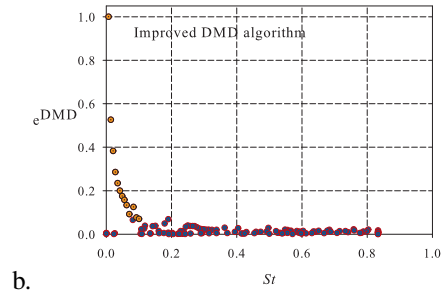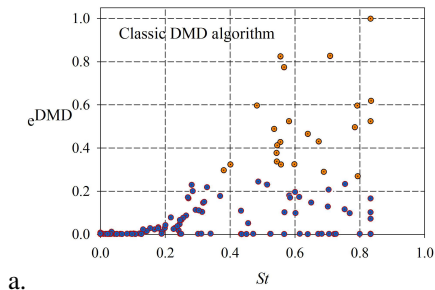$r_{DMD} = 23$ $r_{DMD} = 13$

Figure: Decomposition of streamwise velocity field u-The normalized vector energy versus the Strouhal number: a. Application of classic DMD algorithm; b. Application of improved DMD algorithm - present approach. The lighter colored dots indicate the amplitude values for which the corresponding modes and Ritz eigenvalues are kept in the flow reconstruction.

Second numerical experiment:

$$\Delta t = 1200s, \quad N = 240$$

Spectrum of the Dynamic Mode Decomposition: a. Geopotential field h; b. Streamwise velocity field u; c. Spanwise velocity field v

a.

b.

c.
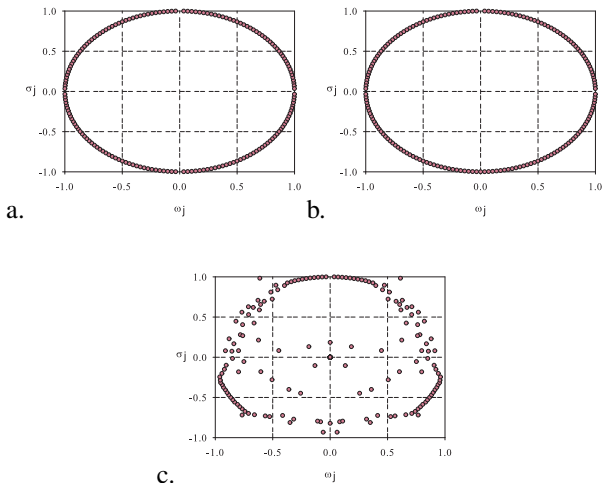
Number of basis functions

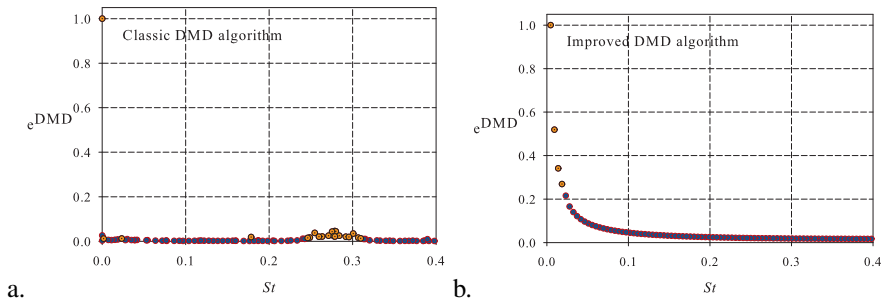$r_{DMD} = 21$ $r_{DMD} = 4$

Figure: The normalized vector energy versus the Strouhal number: The lighter colored dots indicate the modes for which the amplitude values and Ritz eigenvalues are retained in the flow decomposition. a. The classic DMD algorithm - $r_{DMD} = 21$; b. Improved DMD algorithm - present research - $r_{DMD} = 4$, $\Delta t = 1200s$.

Numerical Results for POD Algorithm

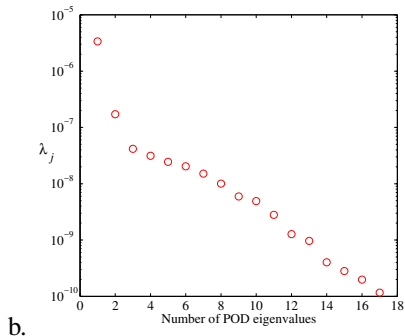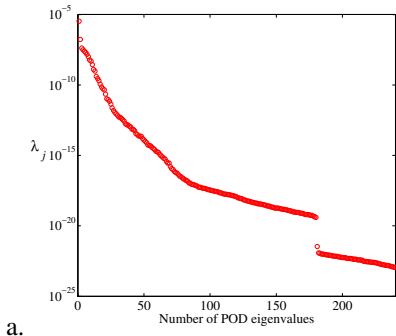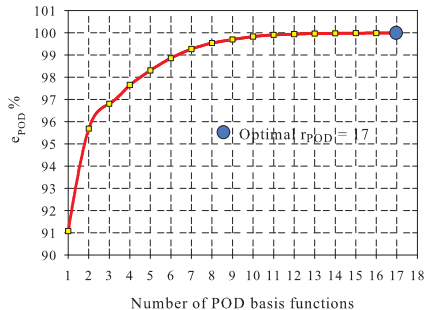Number of basis functions $r_{POD} = 17$

Figure: a. POD eigenvalues; b. Based on an energetic criterion $r_{POD} = 17$ modes are kept for the POD expansion.
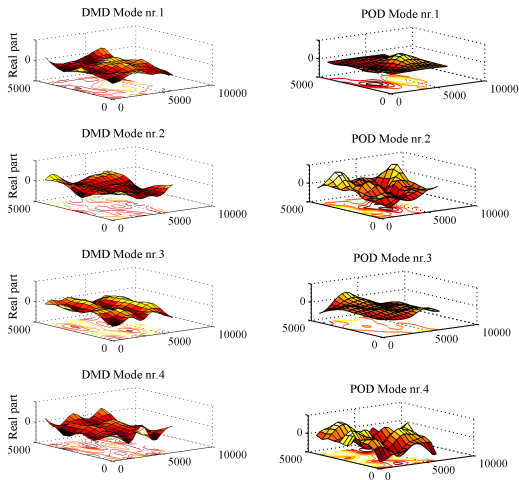
Numerical Results for POD Algorithm

a.

Figure: The energy captured in the POD decomposition as the number of the POD modes.

A Quantitative Comparison of the Spatial Modes

Left: first four DMD modes. Right: first four POD modes.
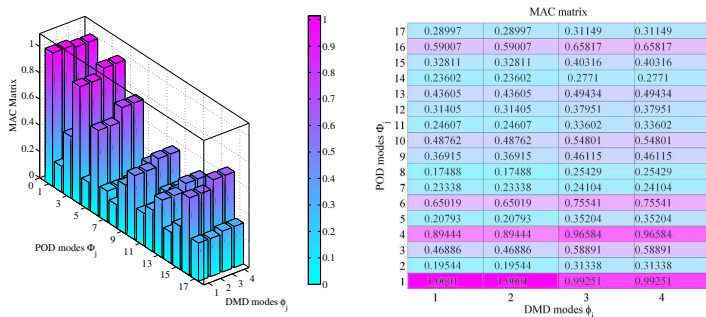
A Quantitative Comparison of the Spatial Modes

MAC matrix			
0.28997	0.28997	0.31149	0.31149
0.59007	0.59007	0.65817	0.65817
0.32811	0.32811	0.40316	0.40316
0.23602	0.23602	0.2771	0.2771
0.43605	0.43605	0.49434	0.49434
0.31405	0.31405	0.37951	0.37951
0.24607	0.24607	0.33602	0.33602
0.48762	0.48762	0.54801	0.54801
0.36915	0.36915	0.46115	0.46115
0.17488	0.17488	0.25429	0.25429
0.23338	0.23338	0.24104	0.24104
0.65019	0.65019	0.75541	0.75541
0.20793	0.20793	0.35204	0.35204
0.89444	0.89444	0.96584	0.96584
0.46886	0.46886	0.58891	0.58891
0.19544	0.19544	0.31338	0.31338
0.99811	0.99811	0.99251	0.99251

Figure: Modal Assurance Criterion - MAC Matrix between DMD and POD modes.

$$MAC_{ij}\left(\phi_i^{DMD}, \Phi_j^{POD}\right) = \frac{\left(\left\|\left(\phi_j^{DMD}\right)^H \cdot \Phi_j^{POD}\right\|_F\right)^2}{\left\|\left(\phi_j^{DMD}\right)^H \cdot \phi_j^{DMD}\right\|_F \left\|\left(\Phi_j^{POD}\right)^H \cdot \Phi_j^{POD}\right\|_F}, \tag{43}$$

The first four DMD modes are sufficient to describe the flow field, as indicated the higher MAC values $\Rightarrow$ DMD is more efficient than POD in term of reduced size of ROM.

Table: The average relative errors of reduced order models

DMD-ROM	POD-ROM
$error_{DMD}^{h} = 0.0119$	$error_{POD}^{h} = 0.0042$
$error_{DMD}^{u} = 0.1770$	$error_{POD}^{u} = 0.0929$
$error_{DMD}^{v} = 0.1534$	$error_{POD}^{v} = 0.0456$

Table: Energy conserving test

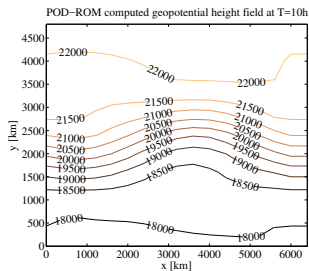| DMD-ROM	POD-ROM
$\left| E - E^{DMD} \right| = 0.1956 \times 10^{-5}$	$\left| E - E^{POD} \right| = 0.7436 \times 10^{-6}$

Comparison of the geopotential height field solution between full model and reduced order models at time $T = 10h$: a. Full solution; b. DMD-ROM solution; c. POD-ROM solution.
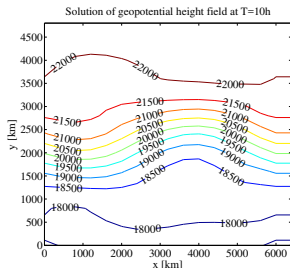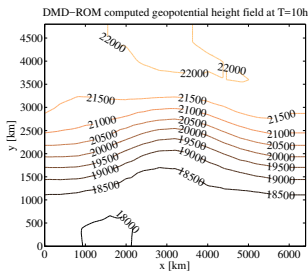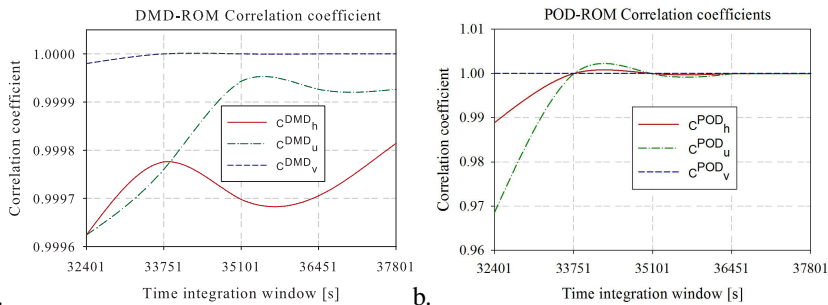
Efficiency of DMD-ROM and POD-ROM Models

Figure: Correlation coefficients for the SWE variables: a. DMD-ROM model vs. full SWE model; b. POD-ROM model vs. full SWE model.
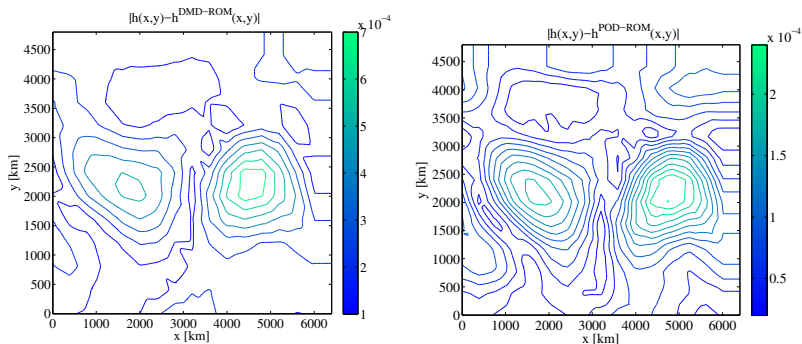
Efficiency of DMD-ROM and POD-ROM Models

Figure: Local errors between DMD-ROM, POD-ROM solutions and the full SWE solution at time $T = 10h$.

Conclusions

(i) Improved DMD method introduced in the present research exhibits more efficiency in reconstruction of flows described by shallow water equations model. For $\Delta t = 1200s$, $r_{DMD} = 4$ Koopman modes are selected for flow reconstruction, while $r_{DMD} = 21$ Koopman modes are retained in the case of the classic DMD algorithm and $r_{POD}=17$ modes are kept for flow reconstruction in POD method.

(ii) By employing the DMD, the most energetic Koopman modes are associated to the the higher amplitudes selected for flow decomposition. Instead, the eigenvalues capturing most of the snapshots energy indicate the corresponding basis functions in POD decomposition.

(iii) DMD is useful when the main interest is to capture the dominant frequency of the phenomenon. POD is useful when the main interest is to find coherent structures in the POD modes which are energetically ranked. Further techniques for system identification or flow optimization can be addressed based on both DMD method and POD method.

Future work

There are a number of interesting directions that arise from this work:

- The application of the proposed algorithm to high-dimensional systems in fluid dynamics and to oceanographic/atmospheric measurements.

- For parametrically varying problems or for modeling problems with strong nonlinearities, the cost of evaluating the reduced order models still depends on the size of the full order model and therefore is still expensive.

- The use of Discrete Empirical Interpolation Method (DEIM) [4] to approximate the nonlinearity in the projection based reduced order strategies for FEM models combined with the methods proposed in this paper.

- The resulting DEIM-DMD-ROM and DEIM-POD-ROM will be evaluated efficiently at a cost that is independent of the size of the original problem.

References

Schmid P. Dynamic mode decomposition of numerical and experimental data. *J. Fluid Mech.* 2010; **656**:5–28.

Koopman B. Hamiltonian systems and transformations in Hilbert space. *Proc. Nat. Acad. Sci.* 1931; **17**:315–318.

Bagheri S. Koopman-mode decomposition of the cylinder wake. *J. Fluid Mech.* 2013; **726**:596–623.

Mezic I. Analysis of fluid flows via spectral properties of the Koopman operator. *Annu. Rev. Fluid Mech.* 2013; **45**(1):357–378.

Rowley CW, Mezic I, Bagheri S, Schlatter P, Henningson DS. Spectral analysis of nonlinear flows. *J. Fluid Mech.* 2009; **641**:115–127.

Belson B, Tu JH, Rowley CW. Algorithm 945: Modred - a parallelized model reduction library. *ACM Transactions on Mathematical Software* 2014; **40**(4):Article 30.

Holmes P, Lumley JL, Berkooz G. *Turbulence, Coherent Structures, Dynamical Systems and Symmetry*. Cambridge Univ. Press., 1996.

References

Navon IM. FEUDX: A two-stage, high accuracy, finite-element Fortran program for solving shallow-water equations. *Computers and Geosciences* 1987; **13**(3):255–285.

Navon IM, DeVilliers R. GUSTAF: a quasi-Newton nonlinear ADI Fortran IV program for solving the shallow-water equations with augmented Lagrangians. *Computers and Geosciences* 1986; **12**:151–173.

Noack BR, Morzynski M, Tadmor G. *Reduced-Order Modelling for Flow Control*. Springer, 2011.

Stefanescu R, Navon IM. POD/DEIM nonlinear model order reduction of an ADI implicit shallow water equations model. *Journal of Computational Physics* 2013; **237**:95–114.

Fang F, Pain CC, Navon IM, Piggott MD, Gorman GJ, Allison P, Goddard AJH. Reduced order modelling of an adaptive mesh ocean model. *International Journal for Numerical Methods in Fluids* 2009; **59(8)**:827–851.

Wang Z, Akhtar I, Borggaard J, Iliescu T. Proper orthogonal decomposition closure models for turbulent flows: A numerical comparison. *Computer Methods in Applied Mechanics and Engineering* 2012; **237-240**:10–26.

Thank You!
D.A. Bistrian, Lecturer, Department of Electrical Engineering and Industrial Informatics, University Politehnica of Timisoara, Romania.
E-mail: diana.bistrian@upt.ro

I.M. Navon, Professor, Department of Scientific Computing, Florida State University, USA.
E-mail: inavon@fsu.edu